



Role of some pyrazol-5-one derivatives as corrosion inhibitors for 316L stainless steel in 1 M HCl

A.S. Fouda*, G.Y. El-Ewady, S. Fathy

Faculty of Science, Department of Chemistry, El-Mansoura University, El-Mansoura 35516, Egypt
Tel. +20 50 2365730; Fax: +20 50 2446254; email: asfouda@mans.edu.eg

Received 21 November 2011; Accepted 5 August 2012

ABSTRACT

The effect of novel, pyrazolone derivatives, namely, (Z)-3-methyl-4-(2-*m*-tolylhydrazono)-1H-pyrazol-5(4H)—compound A, (Z)-4-(2-(3-methoxyphenyl)hydrazono)-3-methyl-1H-pyrazol-5(4H)—compound B, and (Z)-3-methyl-4-(2-(3-nitrophenyl) hydrazono)-1H-pyrazol-5(4H)—compound C as corrosion inhibitors of 316L stainless steel (SS) in 1M HCl has been investigated by using weight loss, potentiodynamic polarization, electrochemical impedance spectroscopy (EIS), and electrical frequency modulation (EFM) techniques. Polarization data clearly indicated that the pyrazol-5-one derivatives behave as mixed type inhibitors. The effect of temperature on corrosion inhibition has been studied and the thermodynamic activation and adsorption parameters were calculated and discussed. EIS was used to investigate the mechanism of corrosion inhibition. EFM can be used as a rapid and nondestructive technique for corrosion rate measurements without prior knowledge of Tafel constants. The adsorption of compounds on 316L SS was found to obey Temkin adsorption isotherm.

Keywords: 316L SS; HCl; EFM; EIS; Pyrazol-5-one derivatives

1. Introduction

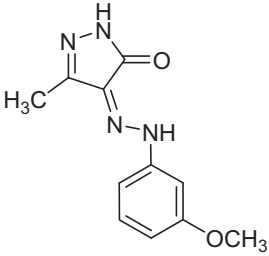
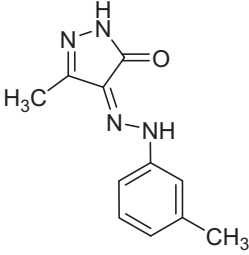
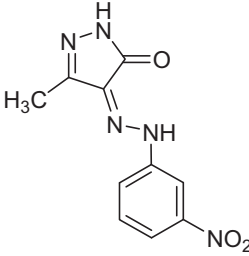
Austenitic stainless steel (SS) are widely used in many applications, where high corrosion resistance is required, such as in the petrochemical and pharmaceutical industries, industrial power generation, and desalination plants. However, certain factors in the handling or manufacturing of these alloys can make them susceptible to localized corrosion and affect their performance. Cleaning and pickling remove foreign materials and promote stability, achieving a uniform surface that is resistant to localized corrosion. SS passivation favors corrosion resistance by forming a protective oxide film [1].

The selection of appropriate inhibitors mainly depends on the type of acid, its concentration and temperature, the presence of dissolved organic and/or inorganic substances, and, of course, on the type of metallic material exposed to the action of the acidic solution [2–4]. Also, cost, toxicity, and availability are important factors in the selection and utilization of these inhibitors. A number of studies have recently appeared in the literature [5–17] on the topic of the corrosion inhibition of 316L SS in acidic media by organic compounds.

The corrosion inhibition of 316L SS becomes of such interest to do because it is widely used as a constructional material in many industries and this is due to its excellent mechanical properties and low cost. So, we try to study its corrosion inhibition in HCl using some new pyrazol-5-one derivatives by different techniques.

*Corresponding author.

Table 1
The chemical structure of the investigated pyrazol-5-one derivatives

Compounds	Structure	Name	Formula & Molecular Weight
A		(Z)-4-(2-(3-Methoxy phenyl)hydrazono)-3-ethyl-1H-pyrazol-5(4H)-one	C ₁₁ H ₁₂ N ₄ O ₂ 232.24
B		(Z)-3-Methyl-4-(2-m-tolyl hydrazono)-1H-pyrazol-5(4H)-one	C ₁₁ H ₁₂ N ₄ O 216.24
C		(Z)-3-Methyl-4-(2-(3-nitro phenyl)hydrazono)-1H-pyrazol-5(4H)-one	C ₁₀ H ₉ N ₅ O ₃ 247.21

2. Experimental detail

316L SS used in this study had the following chemical composition in weight % C 0.02, Mn 1, P 0.054, S 0.02, Si 1, Cr 16, Ni 11, Mo 3, Cu 0.2, and the remaining was Fe.

AnalaR grade 37% HCl and bidistilled water were used to prepare all the solutions. All the experiments were performed at 25°C.

The inhibitors were synthesized in the laboratory according to a previously described experimental procedure, [18] purified and characterized by nuclear magnetic resonance and infrared spectroscopy, and elemental analysis was performed before use. The structure formula of the inhibitors examined is given in (Table 1).

Weight loss measurements were performed on 316L SS coupons, with dimensions 2 × 2 × 0.2 cm, in 1 M HCl solution with different concentrations of the inhibitor. The coupons were abraded with a series of

emery papers of different grit sizes up to 1,200, dried and weighed, and then suspended in 100 ml solution of HCl with and without different concentrations of the studied inhibitors for the exposure period of 3 h at the temperature range from 25 to 55°C. At the end of the tests, the coupons were rinsed with distilled water, degreased with acetone, washed thoroughly again with bidistilled water, dried using filter papers, and weighed again. Experiments were carried out in triplicate to get good reproducibility.

Electrochemical experiments used 316L SS specimen of the same composition which was mounted on a glass rod with an exposed area of 1 cm². An epoxy resin was used to fill the space between the glass rod and the 316L SS electrode. The electrochemical measurements (potentiodynamic polarization, electrochemical impedance spectroscopy (EIS), and electrochemical frequency modulation (EFM) techniques) were performed in a conventional three-electrode

glass cell with 316L SS specimen as working electrode, platinum sheet as counter electrode, and a saturated calomel electrode (SCE) as the reference electrode. Prior to each experiment, the electrode was treated as in weight loss measurements. The electrode potential was allowed to stabilize for 30 min before starting the measurements. For potentiodynamic polarization, the electrode potential automatically changed from -600 to $+400$ mV vs. open circuit potential (E_{OCP}) with a scan rate of 5 mV s^{-1} . For EIS measurements, experiments were conducted in the frequency range of 100 – 10 mHz at the open circuit potential (OCP). The amplitude was 5 mV. For EFM measurements, experiments were carried out using two frequencies, 2 and 5 Hz. The base frequency was 1 Hz with 32 cycles, so the waveform repeats after 1 s. A perturbation signal with amplitude of 10 mV was used. The choice for the frequencies of 2 and 5 Hz was based on three principles [19].

Electrochemical measurements were performed with a Potentiostat/Galvanostat/ZRA (Gamry PCI 300/4) and a personal computer with DC105 software for DC corrosion measurements, EIS300 software for EIS measurements, and EFM140 software for EFM measurements. Echem Analyst software 5.1 was used for plotting, graphing, and fitting data. The measurements were carried out at 25°C .

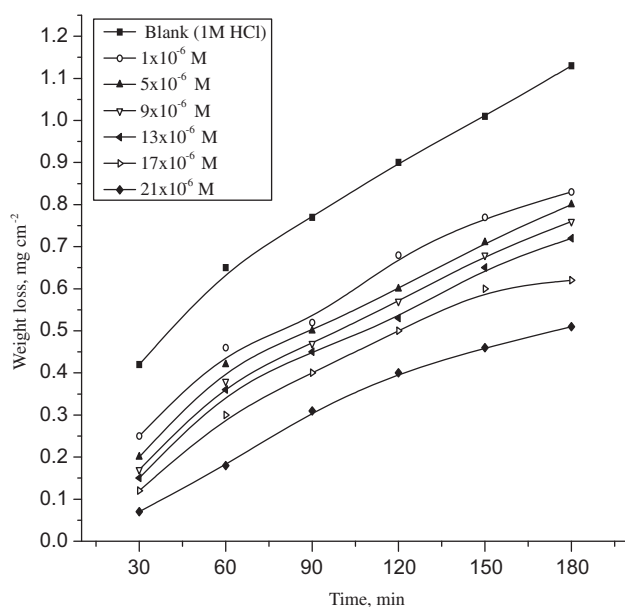


Fig. 1. Weight loss–time curves for the dissolution of 316L SS in the absence and presence of different concentrations of compound A in HCl at 25°C .

Table 2

Inhibition efficiency ($\% \eta$) of the corrosion of 316L SS in 1 M HCl in the presence of different concentrations of pyrazol-5-one derivatives at 25°C and for 90 min immersion

Conc. (M)	Inhibition efficiency ($\% \eta$)		
	A	B	C
1×10^{-6}	29	26	20
5×10^{-6}	35	31	28
9×10^{-6}	41	38	35
13×10^{-6}	44	41	38
17×10^{-6}	54	49	46
21×10^{-6}	72	60	54

3. Results and discussion

3.1. Weight loss measurements

To elucidate the mechanism of inhibition and to determine the thermodynamic parameters of the corrosion process, weight loss measurements were performed from 25 to 55°C . Weight loss of 316L SS was determined, at various time intervals in the absence and presence of different concentrations of pyrazol-5-one derivatives (A–C). The obtained weight loss–time curves are represented in (Fig. 1) for inhibitor A, the most effective one. Similar curves were obtained for other inhibitors (not shown).

The curves obtained in the presence of inhibitors fall significantly below that of free acid. In all cases, the increase in the inhibitor concentration was accompanied by a decrease in weight loss and an increase in the percentage inhibition. These results led to the conclusion that, these inhibitors are fairly efficient inhibitors for 316L SS dissolution in HCl solution. The degree of surface coverage (θ) and the inhibition efficiency ($\% \eta$) were calculated using the following equation:

$$\% \eta = \theta \times 100 = \left[1 - \left(\frac{\Delta W_{\text{inh}}}{\Delta W_{\text{free}}} \right) \right] \times 100 \quad (1)$$

where ΔW_{inh} and ΔW_{free} are the weight losses per unit area in the presence and absence of the inhibitor, respectively.

The values ($\% \eta$) obtained for pyrazol-5-one derivatives at different concentrations and at 25°C are summarized in (Table 2).

Careful inspection of these results showed that, at the same inhibitor concentration, the order of inhibition efficiency was as follows: $A > B > C$.

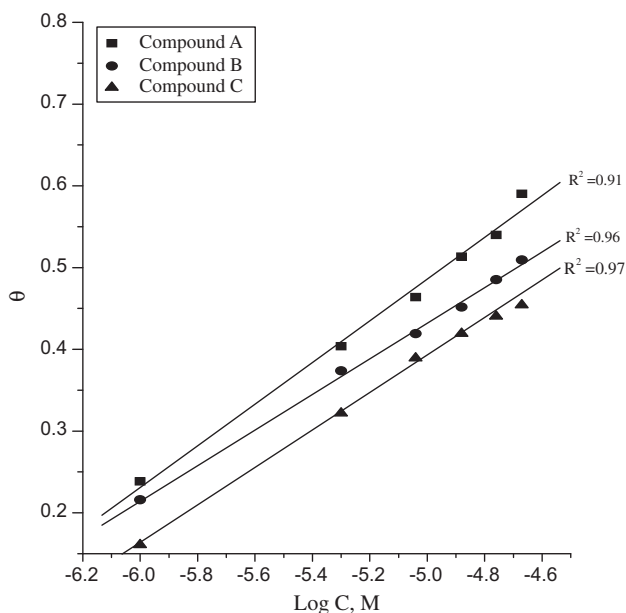


Fig. 2. Temkin adsorption isotherm plotted as θ vs. $\log C$ for the investigated inhibitors of 316L SS in 1M HCl solution from weight loss method at 25°C.

3.2. Adsorption isotherm behavior

The nature of corrosion inhibition has been deduced in terms of the adsorption characteristics of the inhibitors. Metal surface in aqueous solution is always covered with adsorbed water dipoles. Therefore, adsorption of inhibitor molecules from aqueous solution is a quasi-substitution process. The degree of surface coverage (θ) for different concentrations of the inhibitors has been evaluated from weight loss measurements. The data were tested graphically by fitting to various isotherms. A straight line with correlation coefficient nearly equal to 1.0 ($R^2 > 0.9$) was obtained on plotting θ against $\log C$ suggesting that the adsorption of pyrazol-5-one derivatives on SS surface followed Temkin adsorption isotherm model (Fig. 2). According to this isotherm, the surface coverage is related to the inhibitor concentration by:

$$KC = \exp(-2a\theta) \quad (2)$$

where “ a ” is the molecular interaction parameter and K is the equilibrium constant of the adsorption process.

The free energy of adsorption, $\Delta G_{\text{ads}}^\circ$ was calculated from the following equation:

$$\Delta G_{\text{ads}}^\circ = -RT \ln (55.5 K) \quad (3)$$

where 55.5 is the concentration of water in mol l^{-1} in the solution, R is the universal gas constant, and T is the absolute temperature.

The standard free energy for adsorption was calculated using Eq. (3), where one molecule of water is replaced by one molecule of the inhibitor [20]. The values of $\Delta G_{\text{ads}}^\circ$ and K are given in (Table 3). The negative sign of $\Delta G_{\text{ads}}^\circ$ indicates that the adsorption of these inhibitors on SS surface is a spontaneous process. Generally, the magnitude of $\Delta G_{\text{ads}}^\circ$ around -20 kJ mol^{-1} or less negative indicates electrostatic interaction between inhibitor and the charged metal surface (i.e. physisorption). Those around -40 kJ mol^{-1} or more negative are indicative of charge sharing or transferring from the inhibitor molecules to the metal surface to form a coordinate type of bond (i.e. chemisorptions) [21,22]. In the present work, the calculated values of the free energy of these inhibitors (Table 4) are -20 kJ mol^{-1} or less which indicated that adsorption of these inhibitors on SS surface takes place via physisorption. Large values of K_{ads} mean better inhibition efficiency of the inhibitors, i.e. strong electrical interaction between the double layer existing at the phase boundary and the adsorbing inhibitor molecules (which is in our case). Small values of K_{ads} , however, reveal that such interactions between adsorbing inhibitor molecules and the metal surface are weaker, indicating that the inhibitor molecules are easily removable by the solvent molecules from the metal surface [23].

3.3. Effect of temperature

The temperature is the accelerating factor in most of chemical reactions. It increases the energy of the reacted species, as a result chemical reaction gets much faster. The corrosion reaction is a chemical reaction in which the Fe atoms at the metal surface react with the negatively charged anions (OH^- , SO_4^{2-} , Cl^- , etc.). Hence, increasing the temperature of the environment increases the activation energy of the Fe

Table 3
Equilibrium constant (K_{ads}) and adsorption free energy ($\Delta G_{\text{ads}}^\circ$) for the adsorption of inhibitors on 316L SS in 1M HCl from weight loss method at 25°C

Inhibitors	Temkin adsorption isotherm	
	$K_{\text{ads}} \times 10^{-4} (\text{M}^{-1})$	$-\Delta G_{\text{ads}}^\circ (\text{kJ mol}^{-1})$
A	1,000	21.7
B	178	19.8
C	148	19.5

Table 4

Thermodynamic activation parameters for the dissolution of 316L SS in 1 M HCl in the absence and presence of different concentration of the investigated inhibitors

Inhibitors	Conc. (M)	E_a^* (kJ mol ⁻¹)	ΔH^* (kJ mol ⁻¹)	$-\Delta S^*$ (J mol ⁻¹ K ⁻¹)
Blank	1 M HCl	5.52	2.97	275.8
A	1×10^{-6}	7.15	4.59	273.9
	5×10^{-6}	7.38	4.82	273.2
	9×10^{-6}	7.62	5.07	273.0
	13×10^{-6}	7.14	6.41	270.8
	17×10^{-6}	9.66	7.11	268.6
	21×10^{-6}	18.47	15.94	242.5
B	1×10^{-6}	7.98	5.45	269.92
	5×10^{-6}	7.31	4.79	269.92
	9×10^{-6}	8.72	6.20	268.98
	13×10^{-6}	7.96	5.42	260.02
	17×10^{-6}	8.97	6.44	252.91
	21×10^{-6}	11.55	13.70	235.90
C	1×10^{-6}	7.22	4.67	272.1
	5×10^{-6}	7.21	4.66	272.9
	9×10^{-6}	8.06	5.50	270.8
	13×10^{-6}	7.62	5.07	269.7
	17×10^{-6}	9.12	6.57	268.1
	21×10^{-6}	11.75	8.02	265.2

atoms at the metal surface and accelerates the corrosion process of SS in the acidic media.

The effect of temperature on the corrosion inhibition efficiencies of the tested inhibitors was determined in the absence and presence of different inhibitors at concentration in the range of 1×10^{-6} – 21×10^{-6} M at 25–55°C. For examining the effect of

temperature on the corrosion of SS in the presence of studied inhibitors in 1 M HCl solution, Arrhenius Eq. (4) was used [24].

Arrhenius type plot:

$$k = A \exp\left(\frac{-E_a^*}{RT}\right) \quad (4)$$

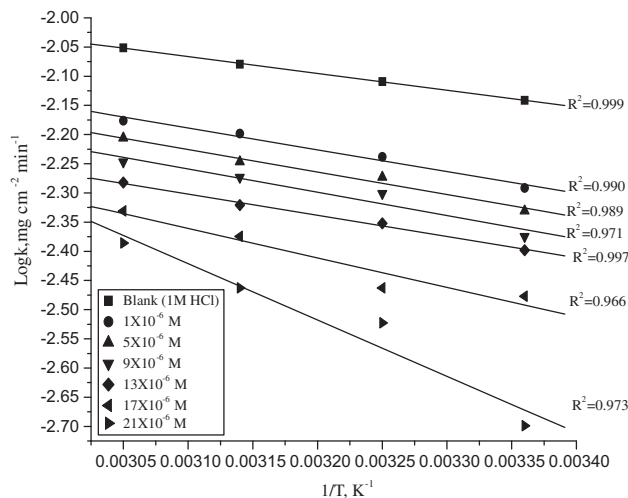


Fig. 3. Arrhenius plots ($\log k$ vs. $1/T$) for the corrosion of 316L SS in 1 M HCl in the absence and presence of different concentrations of inhibitor A.

where, E_a^* is the apparent activation energy and A is the frequency factor.

Plots of $\log k$ (corrosion rate) against $1/T$ (Fig. 3) for 316L SS in 1 M HCl gave straight lines with a slope of $-E_a^*/2.303R$ at which the activation energies were calculated and are represented in (Table 4).

Activation parameters for corrosion of 316L SS were calculated from transition state type equation:

$$k = \frac{RT}{Nh} \exp\left(\frac{\Delta S^*}{R}\right) \exp\left(\frac{-\Delta H^*}{RT}\right) \quad (5)$$

The relation between $\log k/T$ and $1/T$ gives straight lines (Fig. 4), from their slopes and intercepts, ΔH^* and ΔS^* can be calculated and their values are represented in (Table 5).

The results of (Table 5) reveal that, the presence of inhibitors increases the activation energies of 316L SS

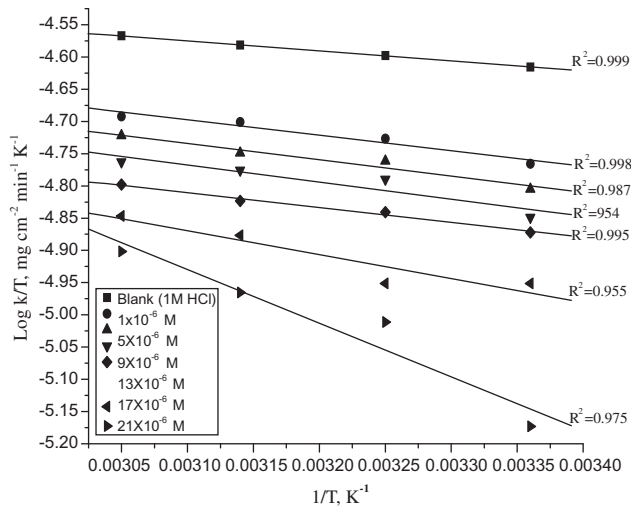


Fig. 4. Plots of $(\log k/T)$ vs. $1/T$ for the corrosion of 316L SS in 1M HCl in the absence and presence of different concentrations of inhibitor A.

indicating strong adsorption of the inhibitor molecules on the metal surface and the presence of these additives induces energy barrier for the corrosion reaction and this barrier increases with increasing inhibitor concentrations. Higher values of activation energy means lower reaction rate and the vice versa is also true. The increase in activation energy with inhibitor concentration is often interpreted by physical adsorption with the formation of an adsorptive film of an electrostatic character [25]. Values of ΔH^* are positive. This indicates that the corrosion process is an endothermic one. The entropy of activation is large and negative. This implies that the activated complex represents association rather than dissociation step, indicating that a decrease in disorder takes place, from reactants to the activated complex [26].

3.4. Electrochemical measurement

3.4.1. Potentiodynamic polarization measurements

Polarization measurements were carried out to obtain Tafel plots in the absence and presence of various concentrations of the inhibitors. (Fig. 5) shows the polarization curves in the absence and presence of inhibitor A. Similar curves were obtained for other inhibitors (not shown). It is observed that the current density of the anodic and cathodic branch is displaced towards lower values. This displacement is more evident with the increase in concentration of the inhibitors when compared to the blank material. The electrochemical parameters of corrosion, such as corrosion current density j_{corr} , corrosion potential E_{corr} ,

corrosion rate CR , anodic Tafel constants β_a , cathodic Tafel constants β_c , and inhibition efficiency η_{Tafel} (%), are given in (Table 5). The inhibition efficiency (η_{Tafel} %) was calculated from polarization curves as follows [8]:

$$\eta_{\text{Tafel}} \% = \left[1 - \frac{j_{\text{corr}}}{j_{\text{corr}}^{\circ}} \right] \times 100 \quad (6)$$

where j_{corr}° and j_{corr} correspond to uninhibited and inhibited corrosion current densities, respectively.

It appears that the inhibition occurred by a blocking mechanism on the available metal spaces [11]. The corrosion potential displayed small change <40 mV around the corrosion potential of -400 mV. These results indicated that the presence of inhibitors affect both SS dissolution and hydrogen evolution; consequently these inhibitors can be classified as mixed corrosion inhibitors.

According to the results in Table 5, the order of the inhibition efficiency was as follows: $A > B > C$. It is important to note that there exists a difference in inhibition efficiency determined by weight loss and polarization methods. This may be, due to the longer time taken in the case of weight loss (3 h) than in the case of polarization method (30 min after reaching OCP).

3.4.2. Electrochemical impedance spectroscopy

EIS measurements were carried out at 25°C in acid solution with and without inhibitors. (Fig. 6) shows the typical EIS diagrams obtained in 1M HCl with and without inhibitor A. The charge transfer resistance (R_{ct}) is calculated from the difference in impedance at lower and higher frequencies. The double layer capacitance (C_{dl}) and the frequency at which the imaginary component of impedance is maximal ($-Z_{\text{max}}$) are found as follows:

$$C_{\text{dl}} = \frac{1}{2\pi f \cdot R_{\text{ct}}} \quad (7)$$

The equivalent circuit that describes our metal/electrolyte interface is shown in (Fig. 7), where, R_s , R_{ct} , and CPE refer to solution resistance, charge transfer resistance, and constant phase element, respectively. EIS parameters and ($\% \eta$) were calculated and tabulated in (Table 6). As we notice, (Fig. 6)—the impedance diagrams—consists of one large capacitive loop. In fact, the presence of inhibitors enhances the value of R_{ct} in acidic solution indicating a charge-transfer process mainly controlling the corrosion of SS. The increase in R_{ct} values, and consequently of

Table 5 Electrochemical kinetic parameters obtained from potentiodynamic polarization technique for the corrosion of 316L SS in 1M HCl at different concentrations of the investigated inhibitors at 25°C

Inhibitors	Conc. (M)	$-E_{corr}$ mV, vs. SCE	$j_{corr} \times 10^{-4}$ (mA cm ⁻²)	β_c (mV dec ⁻¹)	β_a (mV dec ⁻¹)	R_p (Ω cm ²)	θ	% η	CR (mm y ⁻¹)
Blank	1	397	36.2	109	94	313	–	–	161.3
A	1×10^{-6}	394	20.1	107	86	546	0.400	40.0	89.83
	5×10^{-6}	393	8.4	110	79	1,260	0.770	77.0	37.64
	9×10^{-6}	397	7.2	108	76	1,426	0.800	80.0	31.92
	13×10^{-6}	400	4.1	86	62	2023	0.900	90.0	17.74
B	17×10^{-6}	389	2.0	93	57	4,068	0.960	96.0	8.002
	1×10^{-6}	402	31.9	106	98	365	0.125	12.0	142.4
	5×10^{-6}	399	20.4	110	77	511	0.430	43.0	91.14
	9×10^{-6}	414	8.6	97	93	1,271	0.770	77.0	38.26
C	13×10^{-6}	407	6.7	92	114	1,735	0.810	81.0	30.06
	17×10^{-6}	365	2.1	105	78	3,908	0.940	94.0	9.15
	1×10^{-6}	400	3.27	108	93	351	0.110	11.0	145.9
	5×10^{-6}	391	21.9	99	83	475	0.400	40.0	97.74
	9×10^{-6}	388	19.9	110	71	958	0.470	47.0	88.67
	13×10^{-6}	382	16.2	112	73	1,255	0.550	55.0	72.34
	17×10^{-6}	388	12.9	97	76	1,521	0.640	64.0	57.63

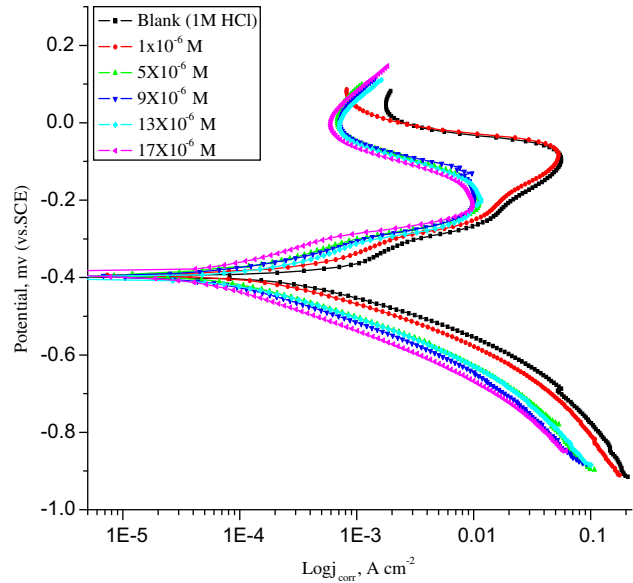


Fig. 5. Potentiodynamic polarization curves for the dissolution of 316L SS in 1M HCl in the absence and presence of different concentrations of inhibitor A at 25°C.

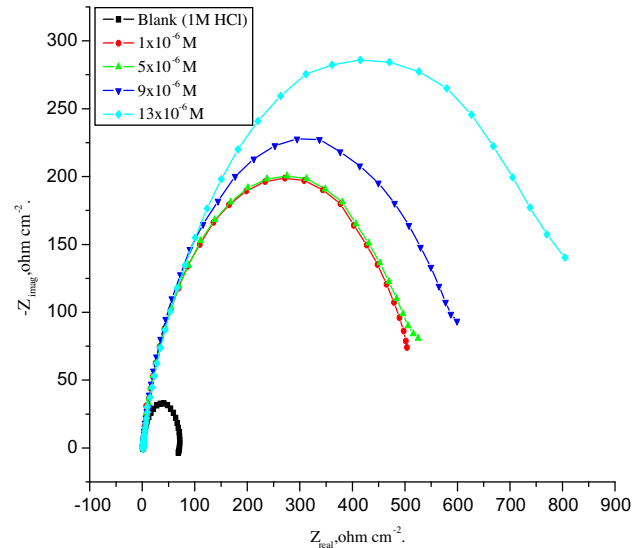


Fig. 6. The Nyquist plots for 316L SS in 1M HCl solution in the absence and presence of different concentrations of inhibitor A at 25°C.

inhibition efficiency, may be due to the gradual replacement of water molecules by the adsorption of the inhibitor molecules on the metal surface to form an adherent film on the metal surface and this suggests that the coverage of the metal surface by the film decreases the double layer thickness. Values of double layer capacitance decrease to the maximum extent in the presence of inhibitors. This decrease of C_{dl} at the

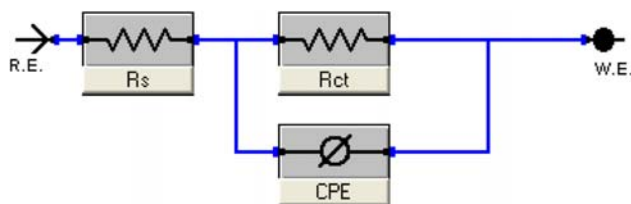


Fig. 7. Electrical equivalent circuit used to fit the impedance data for 316L SS in 1 M HCl solution.

metal/solution interface with increase in the inhibitor concentration can result from a decrease in local dielectric constant which indicates that the inhibitors were adsorbed on the surface at both anodic and cathodic sites [27].

Deviation from perfect circuit shape is often referred to the frequency dispersion of interfacial impedance. This anomalous phenomenon is generally attributed to the inhomogeneity of the metal surface arising from surface roughness or interfacial phenomena [28,12].

The impedance data confirm the inhibition behavior of the inhibitors obtained with other techniques. From the data of (Table 6), it can be seen that the j_{corr} values decrease significantly in the presence of these additives and the (% η) is greatly improved. The order of reduction in j_{corr} exactly correlates with that obtained from potentiostatic polarization studies. Moreover, the decrease in the values of j_{corr} follows the same order as that obtained for the values of C_{dl} . It can be concluded that the inhibition efficiency found from weight loss, polarization curves, and elec-

trochemical impedance spectroscopy measurements are in good agreement.

3.4.3. Electrochemical frequency modulation

Bosch et al. recently proposed EFM as a new electrochemical technique for online corrosion monitoring [6,13,29,30]. EFM is a rapid and nondestructive corrosion rate measurement technique that can directly give values of the corrosion current without prior knowledge of Tafel constants.

In corrosion research, it is known that the corrosion process is nonlinear in nature, a potential distortion by one or more sine waves will generate responses at more frequencies than the frequencies of applied signal. Virtually, no attention has been given to the intermodulation or electrochemical frequency modulation. However, EFM showed that this nonlinear response contains enough information about the corroding system so that the corrosion current can be calculated directly. The great strength of the EFM is the causality factors that serve as an internal check on the validity of the EFM measurement [19]. With the causality factors, the experimental EFM data can be verified.

Figs. 8–12 show that the current response contains not only the input frequencies, but also contains frequency components which are the sum, difference, and multiples of the two input frequencies.

The larger peaks were used to calculate the corrosion current density (j_{corr}), the Tafel slopes (β_a and β_c), and the causality factors (CF-2 and CF-3). These electrochemical corrosion kinetic parameters at different

Table 6

Electrochemical kinetic parameters obtained from EIS technique for the corrosion of 316L SS in 1 M HCl at different concentrations of the investigated inhibitors at 25 °C

Compounds	Conc. (M)	$C_{\text{dl}} \times 10^{-3}$, ($\mu\text{F cm}^{-2}$)	R_{ct} (Ωcm^2)	θ	(% η)
Blank	0.0	14.0	72.2	–	–
A	1×10^{-6}	1.99	508.3	0.857	85.7
	5×10^{-6}	1.96	516.6	0.860	86.0
	9×10^{-6}	1.70	589.7	0.877	87.7
	13×10^{-6}	1.20	789.4	0.908	90.8
B	1×10^{-6}	3.00	335.7	0.785	78.5
	5×10^{-6}	2.80	348.8	0.793	79.3
	9×10^{-6}	2.40	406.7	0.822	82.2
	13×10^{-6}	1.90	532.7	0.864	86.4
C	1×10^{-6}	9.30	107.1	0.423	42.3
	5×10^{-6}	7.60	131.8	0.465	46.5
	9×10^{-6}	7.40	135	0.485	48.5
	13×10^{-6}	6.90	146.4	0.527	52.7

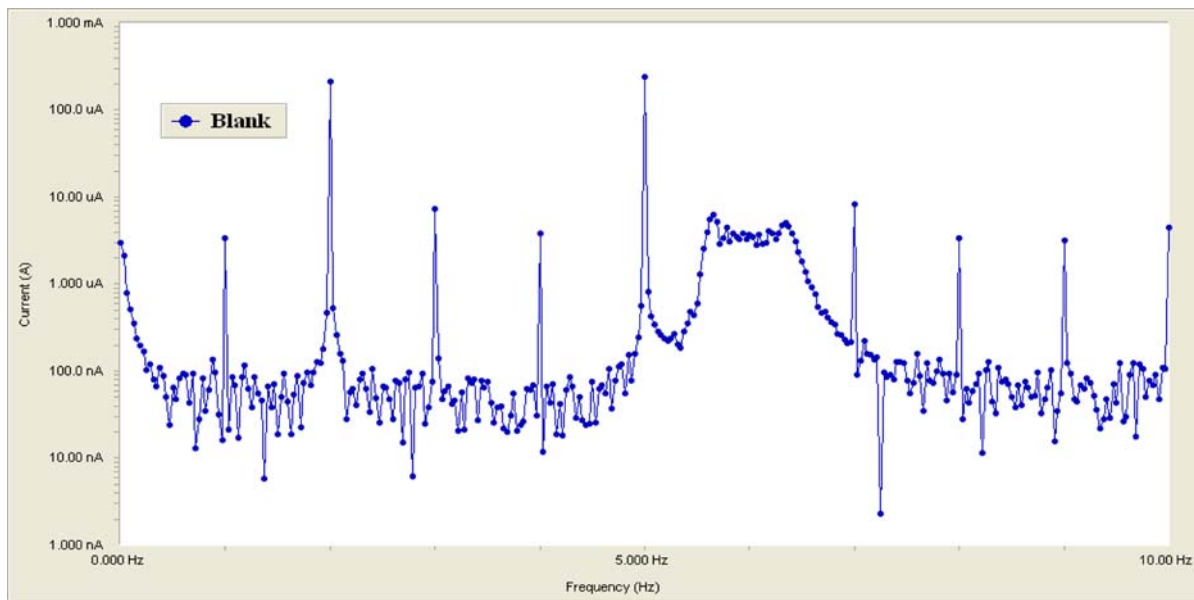


Fig. 8. EFM spectra for 316L SS in 1 M HCl (blank).

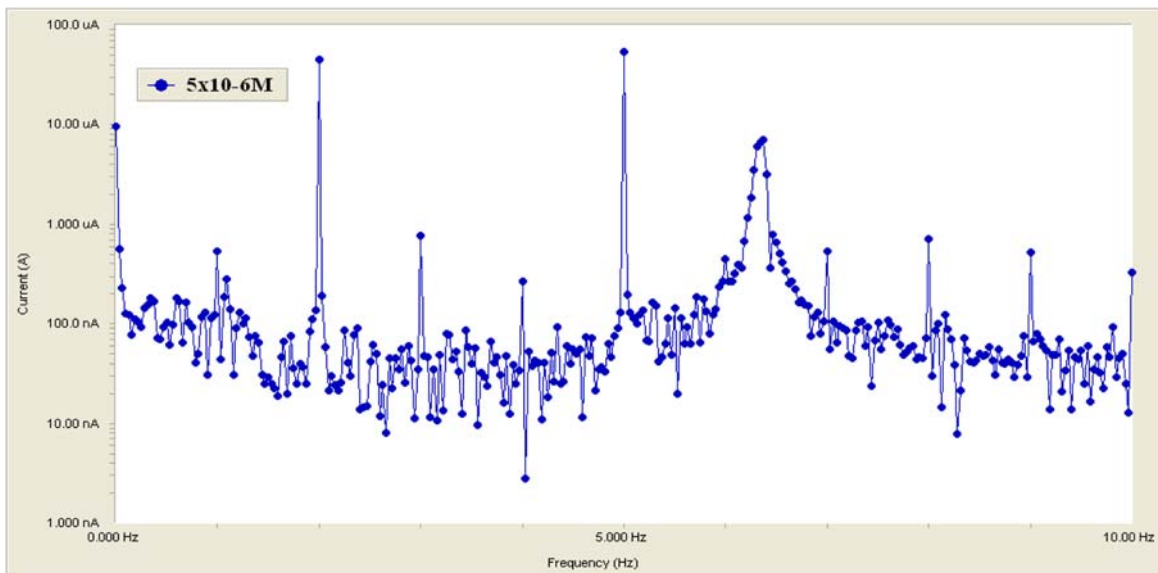


Fig. 9. EFM spectra for 316 L SS in 1 M HCl in the presence of 5×10^{-6} M of inhibitor A.

concentrations of inhibitors in 1 M HCl at 25°C were simultaneously determined and are listed in Table 7.

The inhibition efficiency(% η), calculated from Eq. (6), increases with the increase in concentration of the studied inhibitors.

The causality factors, CF-2 and CF-3, in Table 7 are close to their theoretical values of 2.0 and 3.0, respectively, indicating that the measured data are of good quality.

The calculated inhibition efficiency obtained from weight loss, Tafel polarization, and EIS measurements

are in good agreement with that obtained from EFM measurements.

The difference in inhibition efficiency obtained from the three methods, may be attributed to the different surface status of the electrode in the three measurements, EIS measurements were performed at the rest potential, while in polarization measurements, the electrode potential was polarized to high overpotential, nonuniform current distributions resulting from cell geometry, solution conductivity, counter and ref-

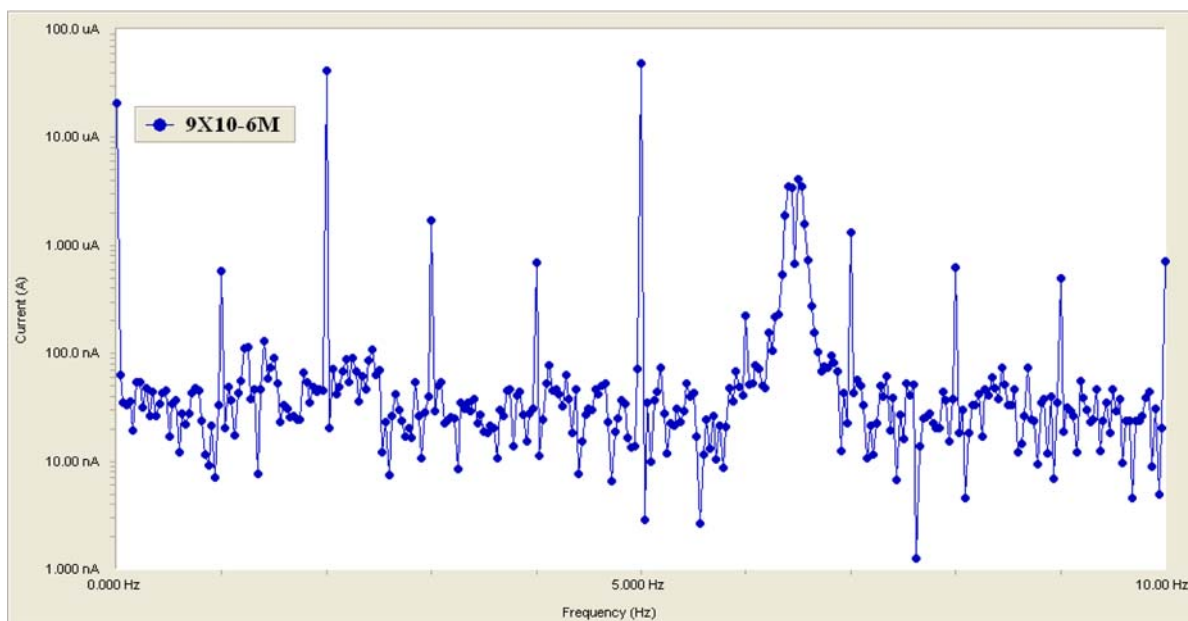


Fig. 10. EFM spectra for 316 L SS in 1 M HCl in the presence of 9×10^{-6} M of inhibitor A.

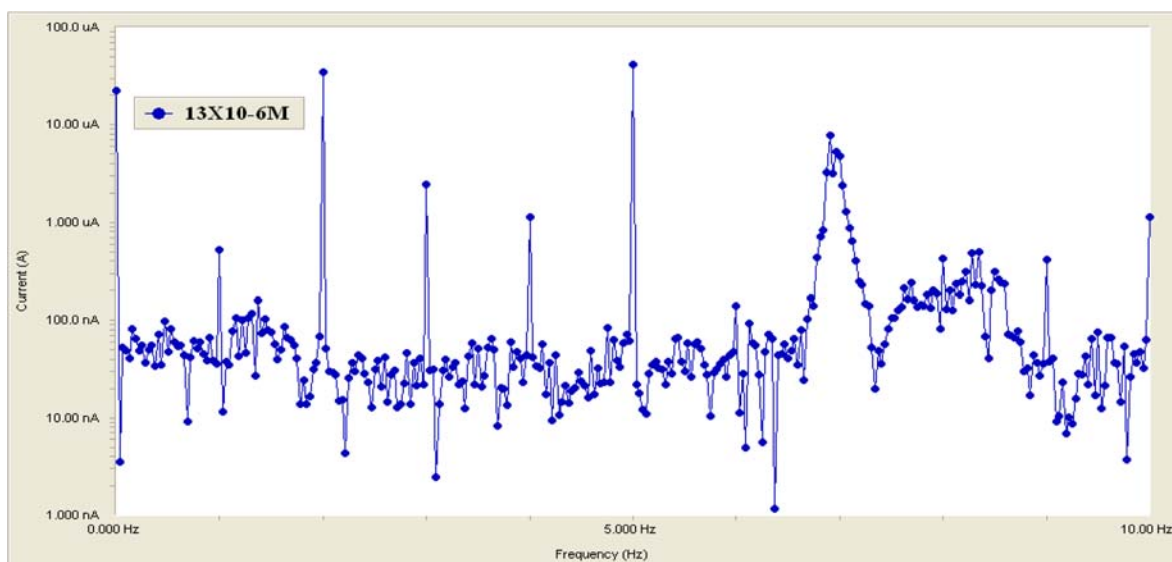


Fig. 11. EFM spectra for 316 L SS in 1 M HCl in the presence of 13×10^{-6} M of inhibitor A.

erence electrode placement, etc. which will lead to the difference between the electrode area [31].

4. Chemical structure and corrosion inhibition

Variation in the structure of inhibitor molecules (A–C) takes place through the pyrazol-5-one derivatives. So, the inhibition efficiency will depend on this part of the molecule.

The weak dependence of the adsorption character of the reaction center of pyrazol-5-one derivatives on the electron density of the ring may be due to the centers of adsorption that are not thoroughly conjugated to the ring.

In general, two modes of adsorption are considered on the metal surface in acid media. In the first mode, the neutral molecules may be adsorbed on the surface of carbon steel through the chemisorption

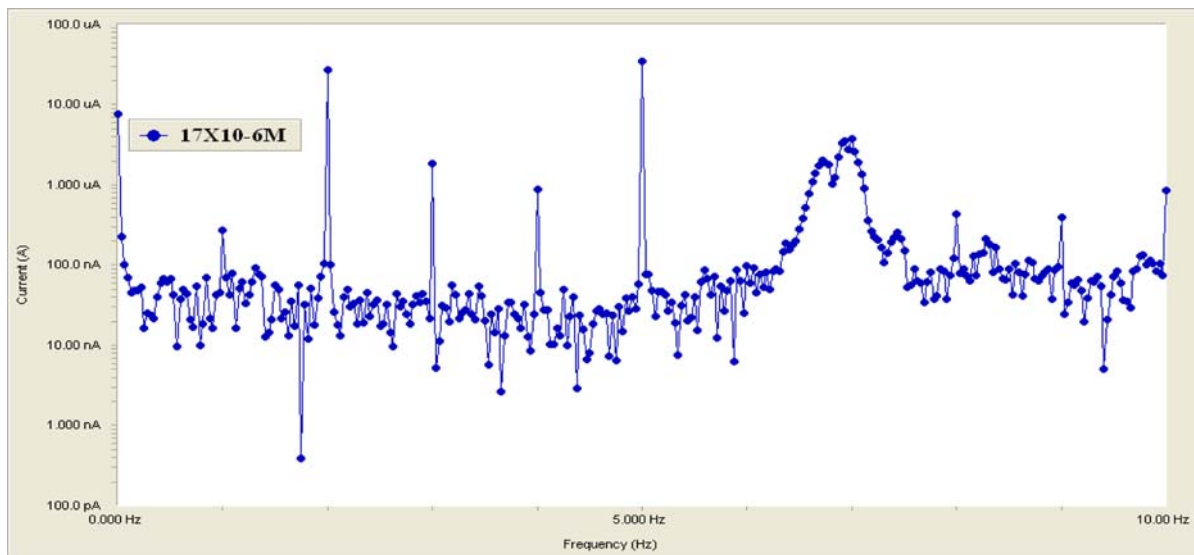


Fig. 12. EFM spectra for 316 L SS in 1 M HCl in the presence of 17×10^{-6} M of inhibitor A.

Table 7

Electrochemical kinetic parameters obtained from EFM technique for 316L SS in 1 M HCl in the absence and presence of different concentrations of the investigated inhibitors

Inhibitors	Conc. (M)	$j_{\text{corr.}}$ ($\mu\text{A cm}^2$)	β_a (mV dec^{-1})	β_c (mV dec^{-1})	CF-2	CF-3	(% η) _{EFM}
Blank	0.0	342.00	88	108	1.9	2.9	–
A	5×10^{-6}	75.20	94	102	2.1	2.8	78.0
	9×10^{-6}	73.53	96	119	2.1	2.7	78.5
	13×10^{-6}	73.37	92	198	2.0	2.9	78.3
	17×10^{-6}	62.40	93	189	2.0	3.0	81.8
B	5×10^{-6}	133.70	92	109	1.9	2.9	61.0
	9×10^{-6}	98.45	91	122	1.9	2.9	71.2
	13×10^{-6}	92.28	84	143	2.0	2.8	73.0
	17×10^{-6}	89.54	88	129	1.9	2.9	74.0
C	5×10^{-6}	201.00	90	105	1.8	2.8	42.0
	9×10^{-6}	196.60	90	104	2.0	2.7	42.5
	13×10^{-6}	183.80	93	107	2.0	2.7	46.3
	17×10^{-6}	171.70	91	107	2.1	2.8	50.0

mechanism, involving the displacement of water molecules from the SS surface and the sharing electrons between the heteroatoms and iron. The inhibitor molecules can also adsorb on the SS surface on the basis of donor–acceptor interactions between π -electrons of the aromatic ring and vacant d-orbitals of surface iron atoms. In the second mode, since it is well known that the SS surface bears positive charge in acid solution [30,31], so it is difficult for the protonated molecules to approach the positively charged SS surface due to the electrostatic repulsion. Since chloride ions have a smaller degree of hydration, thus, they could bring

excess negative charges in the vicinity of the interface and favor more adsorption of the positively charged inhibitor molecules, the protonated pyrazol-5-one derivatives adsorb through electrostatic interactions between the positively charged molecules and the negatively charged metal surface. Thus, there is a synergism between adsorbed Cl^- ions and protonated pyrazol-5-one derivatives. Thus, we can conclude that inhibition of SS corrosion in 1 M HCl is mainly due to the electrostatic interaction. The decrease in the inhibition efficiency with rise in temperature supports electrostatic interaction.

Inhibitor A is the most efficient inhibitor because of: (i) the presence of *m*-OCH₃ group ($\sigma = -0.12$) which enhances the delocalized π -electrons on the molecule, (ii) it also may add an additional active center to the molecule due to its oxygen atom, and also (iii) due to its higher molecular size. Inhibitor B comes after compound A in inhibition efficiency, because of the presence of *m*-CH₃ with $\sigma = -0.07$ which contributes less electron density to the molecule. Inhibitor C is the least efficient inhibitor. This may be due to: (i) Its highest electrophilic character ($\sigma_{\text{NO}_2} = +0.78$) of NO₂ group, (ii) NO₂ may be reduced easily in acid medium, and (iii) the evolved heat of hydrogenation may aid to the desorption of the molecules. According to the previous discussion, the nature of substituted group, whether electron donating or withdrawing, reflects its effect on the inhibition efficiency.

5. Conclusion

The investigated compounds show excellent performance as corrosion inhibitors in HCl solution. The inhibition efficiency of pyrazol-5-one derivatives follows the order: A > B > C. Polarization studies showed that pyrazol-5-one derivatives behave as mixed type inhibitors for SS in HCl solution. Impedance studies indicated that R_{ct} values increased, while C_{dl} values decreased in the presence of the inhibitors. The adsorption of the investigated inhibitors was found to follow the Temkin adsorption isotherm indicating that the inhibition process occurs via adsorption. The % η obtained from weight loss, polarization curves, electrochemical impedance spectroscopy, and electrochemical frequency modulation are in good agreement.

References

- [1] C.D. Dillon, Performance 33 (1994) 62–64.
- [2] W.P. Wang, D. Casta, P. Marcus, J. Electrochem. Soc. 141 (1994) 2669–2671.
- [3] P.Q. Zhang, J.X. Wu, W.Q. Zhang, X.Y. Lu, K. Wang, Corros. Sci. 34 (1993) 1343–1354.
- [4] A. Atrens, B. Baroux, M. Mantel, J. Electrochem. Soc. 144 (1997) 3697–3704.
- [5] Fadda, M.E.A. Zaki, Kh. Samir, F.A. Amsr, Khim. Geterotsiki Soedin (Chem. Heterocycl. Compd.) 9 (2003) 1413–1419.
- [6] R.W. Bosch, J. Hubrecht, W.F. Bogaerts, B.C. Syrett, Corrosion 57 (2001) 60–70.
- [7] D.A. Jones, Principles and Prevention of Corrosion, second ed., Prentice Hall, Upper Saddle River, NJ, 1983.
- [8] M. Kendig, S. Jeanjaquet, J. Electrochem. Soc. 149 (2002) B47–B51.
- [9] F. Mansfeld, M.W. Kendig, S. Tsai, Corrosion 38 (1982) 570–580.
- [10] F. Mansfeld, Electrochim. Acta 35 (1990) 1533–1538.
- [11] E. McCafferty, N. Hackerman, J. Electrochem. Soc. 119 (1972) 146–154.
- [12] K.F. Khaled, Int. J. Electrochem. Sci. 3 (2008) 462–475.
- [13] K.F. Khaled, Electrochim. Acta 53 (2008) 3484–3492.
- [14] W. Huilong, Z. Jiashen, L. Jing, Anti-Corros. Meth. Mater 9(2) (2002) 127–132.
- [15] M.T. Said, S.A. Ali, S.U. Rahman, Anti-Corros. Meth. Mater. 50(3) (2003) 201–207.
- [16] Atia, M.M. Saleh, J. Appl. Electrochem. 33(2) (2003) 171–177.
- [17] S. Tamilselvi, S. Rajeswari, Anti-Corros. Meth. Mater. 50(3) (2003) 223–231.
- [18] H.Tawfik, Evaluation of the inhibition role for some organic compounds in controlling the corrosion of some alloys used in water circuits of steam power plants, Ph.D.Thesis, Ain Shams University, Egypt, 2008.
- [19] I. O'MBockris, D.A. Swinkles, J. Electrochem. Soc. 111 (1964) 736–742.
- [20] F.M. Donahue, K. Noor, J. Electrochem. Soc. 112 (1965) 886–891.
- [21] E. Kamis, F. Bellucci, R.M. Latanision, E.S. El-Ashry, Corrosion 47 (1991) 677–686.
- [22] M.A. Amin, S.S. Abd El-Rehim, M.M. El-Naggar, H.T. Abd El-Fattah, J. Mater. Sci. 44 (2009) 6258–6272.
- [23] E.E. Oguzie, Mater. Chem. Phys. 99 (2006) 441–446.
- [24] A. Popova, E. Sokolova, S. Raicheva, M. Christov, Corros. Sci. 45 (2003) 33–58.
- [25] A.S. Fouda, G.Y. Elewady, A. El-Askalani, K. Shalaby, Zastita Materijala 51(4) (2010) 205–219.
- [26] K.C. Emergul, M. Hayvalf, Corros. Sci. 48 (2006) 797–812.
- [27] H. Shin, H. Mansfeld, Corros. Sci. 29 (1989) 1235–1246.
- [28] S. Martinez, M. Metikos-Hukovic, J. Appl. Electrochem. 33 (2003) 1137–1142.
- [29] M. Lebrini, M. Lagrenée, M. Traisnel, L. Gengembre, H. Vezin, F. Bentiss, Appl. Surf. Sci. 253 (2007) 9267–9276.
- [30] G.N. Mu, T.P. Zhao, M. Liu, T. Gu, Corrosion 52 (1996) 853–856.
- [31] A.K. Singh, M.A. Qurashi, Corros. Sci. 52 (2010) 1529–1535.